Astron. Astrophys. 330, 381–388 (1998)

ASTRONOMY AND ASTROPHYSICS

Motion of ions reflected off quasi-parallel shock waves in the presence of large-amplitude magnetic field fluctuations

H.-T. Claßen and G. Mann

Astrophysikalisches Institut Potsdam, Observatorium für solare Radioastronomie, Telegrafenberg A31, D-14473 Potsdam, Germany

Received 10 February 1997 / Accepted 17 September 1997

Abstract. We analyse the behaviour of protons reflected off supercritcal, quasi-parallel shock waves in the presence of large amplitude magnetic field fluctuations with a magnetic field compression larger than the background magnetic field ($1 \leq \Delta B/B_0 \leq 2.5$). These so-called SLAMS (short large-amplitude magnetic field structures) have originally been observed in the quasi-parallel region of the earth's bow shock. In general, the characteristics of the particle motion depend on the amplitude, the phase and the propagation direction of the SLAMS convected back to the shock front. Numerically calculated test particle trajectories show that in case of small gyroradii these dependencies reduce to pure geometrical conditions. In this case the computations can be simplified using results from adiabatic theory. Furthermore, it can be seen that the presence of SLAMS prevents the reflected ions from escaping into the upstream region of the shock. Although the shock geometry is quasi-parallel, some of the upstream moving ions return back to the shock front and subsequently penetrate into the downstream region. Because of their reflection at the incoming SLAMS these ions have a larger energy than their starting energy and can thus contribute to downstream heating and thermalisation. As a possible application we present an interpretation of cold ion bunches observed in connection with supercritical, quasi-parallel shock waves.

Key words: shock waves – acceleration of particles – magnetic fields – interplanetary medium

1. Introduction

In magnetohydrodynamics (MHD) shock waves are idealized as discontinuities without any internal structure, while real measurements show a more or less rich inner life of these structures ordered by the shock velocity and geometry (see Kennel et al. 1985, as a review). From a microscopic point of view the difference between quasi-parallel and quasi-perpendicular shock waves can be understood analysing the ion movement. Thus, the simple MHD description of streaming fluids becomes modified because of ion reflections at the shock transition zone. The reasons for reflection are magnetic mirror effects due to magnetic field compressions (e.g. Sonnerup 1969) and/or an electric potential rise inside the transition zone of the shock (e.g. Goodrich & Scudder 1984). The reflection process itself can be described either as adiabatic processes conserving the "magnetic moment" m_M or not m_M-conserving reflections (e.g. specularly reflected ions, Paschmann et al. 1982). For steady, uniform magnetic fields on both sides of the shock the guiding center velocity of ions specularly reflected at the shock transition is directed upstream if the angle between the unperturbed upstream magnetic field and the shock normal $\theta_{B_0 n}$ is smaller than 45° and downstream if $\theta_{B_0 n} > 45°$ (Gosling et al. 1982). For shock waves with $39.9° < \theta_{B_0 n} < 45°$ the gyromotion of the reflected ions causes them to reencounter the shock even though the guiding center velocity is directed upstream (Schwartz et al. 1983).

Most of the information from shock waves in space plasmas comes from the various satellite missions investigating the bow shock of the earth. They found that the upstream region of the bow shock is populated with different types of superthermal ion distributions. At least four distinct classes have been identified: "reflected ions" (Asbridge et al. 1968), "intermediate ions" (Paschmann et al. 1979), "diffuse ions" (Gosling et al. 1978) and "gyrating ions" (Gosling et al. 1982, Eastmann et al. 1981). Furthermore, a variety of low-frequency magnetic field fluctuations are closely related with these different ion populations backstreaming from the bow shock (for a review see Russell & Hoppe 1983).

Gyrating ion distributions are typically associated with large-amplitude monochromatic MHD-like waves (Thomsen 1985) and the diffuse and intermediate protons with ULF (ultra-low-frequencies in the order of $0.1\omega_{cp}$) waves (Paschmann et al. 1979), so-called shocklets (Hoppe et al. 1981) and SLAMS (Schwartz et al. 1992). Shocklets appear as steepened waves with amplitudes in the order of the backgound magnetic field (Hoppe et al. 1981). SLAMS were characterized by Schwartz et al. (1992) as well defined single magnetic structures with large

Send offprint requests to: H.-T. Claßen

amplitudes of about two or more times the background magnetic field and short durations of typically 10 s. Fig. 1 shows the magnetic field and density behaviour at a typical SLAMS measured by the AMPTE/IRM satellite.

The relationship between superthermal ions and the different kinds of waves has been reviewed by Thomsen (1985) from the observational point of view and was analysed by numerical particle simulations of supercritical, quasi-parallel shock waves. Diffuse ions in the far-upstream region generate ULF waves propagating along the ambient magnetic field lines. Because of the super-Alfvénic speed of the solar wind they are convected back to earth. During their approach to the bow shock they steepen into shocklets and subsequently into SLAMS. The numerical simulations of Omidi & Winske (1990) showed that the original polarisation of the small-amplitude waves changes from an elliptical (right-handed in the plasma rest frame) to a linear behaviour. Further simulations (Scholer et al. 1992) also confirmed the observed quasi-planar structure of ULF waves and SLAMS (Mann et al. 1994). An analytical approach describing low frequency plasma waves with finite amplitudes and their steepening into SLAMS was carried out by Malara & Elaoufir (1991) and Mann (1995) using non-linear MHD wave theory. These investigations showed that SLAMS can be regarded as simple magnetohydrodynamic waves, i.e., the magnetic field components can be described as functions of the form $b_i = f_i(x - V_{SL}t)$ $(i = x, y, z)$, where V_{SL} is the propagation velocity of the SLAMS.

Looking at this scenario it should be clear that the aforementioned assumption of a steady uniform magnetic field outside the shock transition zone as assumed by Schwartz et al. (1983) is no longer valid. Some of the ions reflected at the shock transition will be reflected back by the incoming wave structures. Especially, coherent bunches of nearly specularly reflected ions are observed in the supercritical, quasi-parallel region of the earth's bow shock (Gosling et al. 1989). Such reflected ions are not always present and seem to be related with the occurence of density fluctuations with shock like features (Onsager et al. 1990).

The aim of this paper is to study the ion motion in such arrangements of moving magnetic mirrors (SLAMS) to get insight in the basic microphysical processes. Thus, our investigations are closely related to an analysis of Fuselier et al. (1986). In both approaches the scattering magnetic field fluctuations that modify the ion movement at quasi-parallel shock waves are based on plasma wave observations at the earth's bow shock. Fuselier et al. (1986) studied the ion movement of specularly reflected ions under the influence of monochromatic MHD-waves with a finite amplitude ($0.25 \leq b_m/b_0 \leq 1$), while our paper is addressed to steepened wave packets with large amplitudes compared to the background magnetic field ($1 \leq b_m/b_0 \leq 2.5$). In the first case the ions move under a permanent influence of a weak magnetic field perturbation and in the second case the ions are only affected occasionally by the contact with single wave packets. The model for the description of the SLAMS, i.e., the electric and magnetic fields used for our test particle calculations, is presented in the next section. The results of the test particle calculations are presented in Sect. 3, where we also discuss our results in the framework of adiabatic theory. Furthermore, we compare our results with those obtained by Fuselier et al. (1986), discuss the validity of adiabatic theory and try to explain the observed coherent bunches of reflected ions (see Sect. 4).

2. Basic model assumptions

Test particle trajectories in the presence of large amplitude magnetic field fluctuations are obtained by solving the equation of motion for single ions in given electric and magnetic fields of SLAMS in front of quasi-parallel shock waves. The calculations are performed in the shock rest frame under the following assumptions (cf. Fig. 2):

1) The ions are reflected off a plane shock front with vectors $\boldsymbol{B_0}$ (unperturbed upstream magnetic field), $\boldsymbol{n}$ (shock normal) and $\boldsymbol{u_1} = V_{SH}\boldsymbol{n}$ (upstream plasma bulk velocity) lying in the (x,z)-plane.

2) Then, the ions move upstream under the combined influence of the ambient magnetic field $\boldsymbol{B_0}$ and the motional electric field $\boldsymbol{E_0} = -\boldsymbol{u_1} \times \boldsymbol{B_0}$ (along the y-axis) superimposed with the magnetic and electric field of the SLAMS $\boldsymbol{B_{SL}}$ and $\boldsymbol{E_{SL}}$ (i.e., $\boldsymbol{B} = \boldsymbol{B_0} + \boldsymbol{B_{SL}}$ and $\boldsymbol{E} = \boldsymbol{E_0} + \boldsymbol{E_{SL}}$).

3) The SLAMS are considered as planar simple waves moving in the negative x-direction, i.e., the magnetic field components can be described as $B_{SLi} = f_i(x - x_0 + V_{SL}t)$ $(i = x, y, z)$. The inclination ψ between the propagation direction and the unperturbed magnetic field should be smaller than θ (see e.g. Mann et al. 1994). The electric field is computed using Faraday's law $\nabla \times \boldsymbol{E_{SL}} = -\partial \boldsymbol{B_{SL}}/\partial t$.

4) A self consistent generation and modification of the SLAMS by the reflected ions is not taken into consideration.

The equation of motion can be written in dimensionless quantities using natural scales T and L for time- and space-coordinates, where $T := \omega_{cp}^{-1} = m_p/eB_{10}$ is the inverse proton cyclotron frequency (m_p, proton mass and e, elementary charge) and $L := c/\omega_{pp}$ the proton inertial length ($\omega_{pp} = (N_1 e^2/\epsilon_0 m_p)^{1/2}$, proton plasma frequency, N_1, upstream particle number density, c, velocity of light and ϵ_0, dielectric field constant). Thus, we obtain

$$\frac{d^2\boldsymbol{x}}{dt^2} = (c/V_A)\boldsymbol{e} + \boldsymbol{v} \times \boldsymbol{b}\,, \tag{1}$$

with $\boldsymbol{b} = \boldsymbol{B}/B_{10}$ and $\boldsymbol{e} = \boldsymbol{E}/cB_{10}$. The velocity is normalized to the Alfvén velocity $V_A = B_{10}/(\mu_0 m_p N_1)^{1/2}$. Using the geometrical conditions depicted in Fig. 2 the dimensionless upstream magnetic field in the shock rest frame is given by

$$\begin{aligned} b_x &= -\cos\psi \\ b_y &= \quad p \cdot b_{\rm m} \cdot f_y(\xi) \\ b_z &= \quad \sin\psi + b_{\rm m} \cdot f_z(\xi)\,, \end{aligned} \tag{2}$$

with the unperturbed magnetic field as $\boldsymbol{b_0} = (-\cos\psi, 0, \sin\psi)$. The magnetic field of the SLAMS is given by b_y and the second term in the b_z-component, with $\xi = x - x_0 + (V_{SL}/V_A)t$. $b_{\rm m}$ and p ($|p| \leq 1$) denote the maximum field compression and

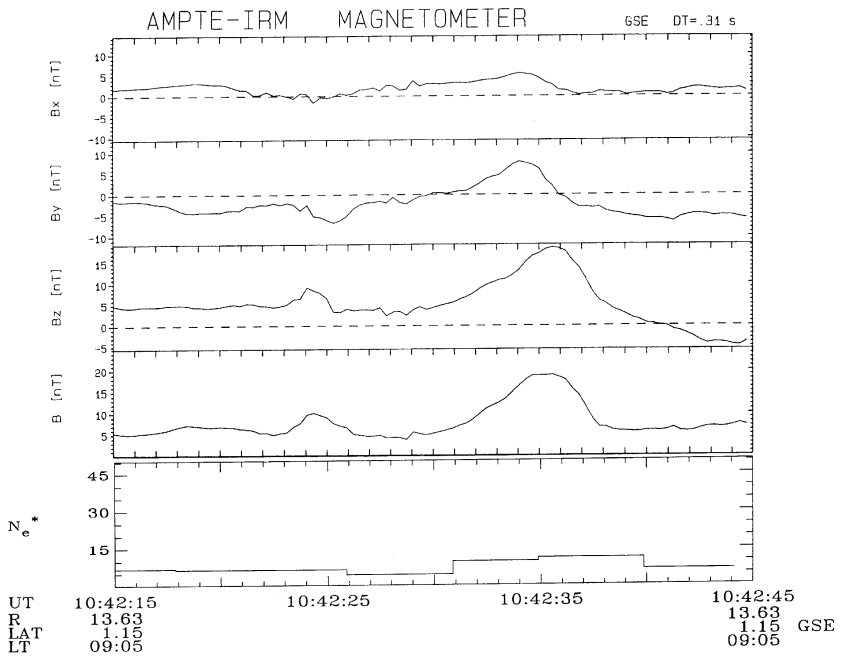

Fig. 1. Magnetic field and density behaviour associated with typical SLAMS occurring on October 30, 1984. The first three panels show the magnetic field components in a minimum variance frame; the fourth panel shows the magnitude of the magnetic field. The fifth panel displays a rise in the electron particle number density associated with the SLAMS (measurement of the AMPTE/IRM satellite).

the polarisation of the SLAMS, respectively. For plane wave structures varying only with the x-coordinate the b_x-component must be a constant because of div $\boldsymbol{b} = 0$. The b_y-term represents a noncoplanar field component of SLAMS. An example for the magnetic field behaviour at SLAMS is shown in Fig. 1.

The dimensionless electric field can be written as a sum of the motional electric field $\boldsymbol{e_0} = -(V_{SH}/c)\boldsymbol{n} \times \boldsymbol{b_{10}}$, superimposed with the electric field $\boldsymbol{e_{SL}}$ induced by the SLAMS motion. Using Faraday's law we obtain

$$\begin{aligned} e_x &= e_x(\xi) \\ e_y &= (V_{SH}/c)\sin\theta - (V_{SL}/c)b_{\rm m} \cdot f_z(\xi) \\ e_z &= (V_{SL}/c)p \cdot b_{\rm m} \cdot f_y(\xi)\,. \end{aligned} \tag{3}$$

The integration constants have been chosen in such a way that the pure motional electric field is obtained outside the SLAMS. Furthermore, it should be noted that the induction equation gives no information about the e_{SLx}-component.

In general, the behaviour of test particles in the electromagnetic fields given by Eqs. 2 and 3 shows two different effects. The first one leads to a small population of clearly superthermal particles accelerated due to the wave electric field parallel to the local magnetic field. Mechanisms of this kind are described for example in Claßen & Mann (1997). Furthermore, the hybrid simulations of Kucharek and Scholer (1991) showed that this process leads to a population of diffusive, superthermal ions, with a ratio of accelerated particles in the order of 1 % . The main effect however is a reflection of the incoming ions with only a slight change of the particle velocity due to a grad-B-drift in the magnetic field of approaching SLAMS. Since we are interested in the behaviour of just this weakly superthermal ions we can simplify our description assuming a vanishing noncoplanar component, i.e., $b_y = 0$ and $\boldsymbol{e} \cdot \boldsymbol{b} = 0$. Thus, we choose $p = 0$ in Eq. 2 and $e_x(\xi) = 0$ in Eq. 3. This assumption is in general not a substantial restriction. Even if we take a polarisation of SLAMS into account the reflection conditions and the energy gained after reflection are not changed. The only effect caused by the noncoplanar component is a energy gain inside the SLAMS (see e.g. Claßen and Mann 1997), but this energy is lost while the particles move out of the SLAMS.

As a special realisation of such modelled SLAMS we took a function f_z given by

$$f_z(\xi) = \begin{cases} \exp(-(\xi/L_1)^2)\cos(k\xi) & \text{if } \xi \geq 0 \\ \exp(-(\xi/L_2)^2)\cos(k\xi) & \text{if } \xi < 0 \end{cases}\,. \tag{4}$$

Here $k = 2\pi/\lambda$ denotes the wave number of the ULF waves (wavelength λ) from which the SLAMS develop and L ($L/\lambda < 1$) is a typical length scale of SLAMS. In correspondence with the statistical analysis of 18 SLAMS observed at the earth's bow shock (Mann et al. 1994) we took $L_1 = 12\,, L_2 = 8$ and $k = 0.1$. Furthermore, the statistical analysis showed that the lateral dimension of SLAMS (y-direction in Fig. 2) is about 100 proton inertial lengths justifying the assumption of SLAMS as plane structures. These scales seem to be typical for steepened wave structures and were confirmed by numerical simulations (e.g. Omidi & Winske 1990, Scholer et al. 1992). Finally, it should be mentioned that the basic results presented in this paper depend on the used length scales and not on the explicit shape of b_z given by Eq. 4 (see Sect. 4).

3. Test particle calculations

In order to solve the equation of motion (Eq. 1) with a magnetic and electric field given by Eqs. 2-4 we used a fourth-order Runge-Kutta method for ordinary differential equations (Press et al. 1992). Starting with a single proton reflected at the shock transition zone and moving back into the upstream region (cf.

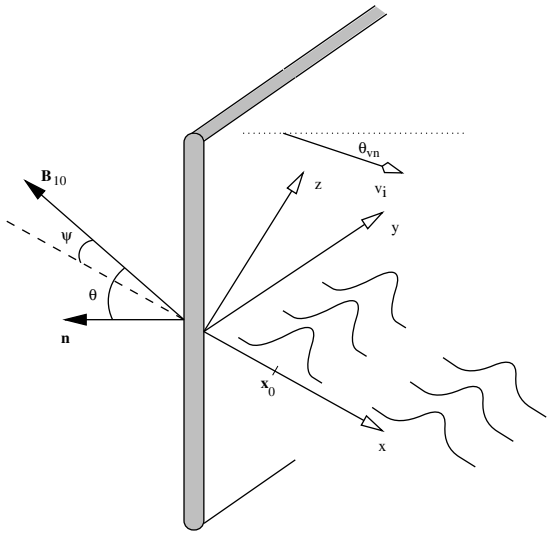

Fig. 2. Geometry of a supercritical, quasi-parallel shock wave with approaching SLAMS in the upstream region: The shock transition zone (grey shaded area) is at rest, the upstream and downstream region are lying at the right and left hand side of this area, respectively. The unperturbed upstream magnetic field $\boldsymbol{B_{10}}$ and the shock normal $\boldsymbol{n}$ spread the (x,z)-plane; x, y, and z are chosen mutually orthogonal. The SLAMS move along the x-axes and are described by their magnetic field compression (b_m, see text) and by their distance x_0 from the transition zone. θ, ψ, and θ_{vn} are the angles between $\boldsymbol{n}$ and $\boldsymbol{B_{10}}$, between the propagation direction of the SLAMS and $\boldsymbol{B_{10}}$, and between the starting velocity $\boldsymbol{v_i}$ of the test particle and $\boldsymbol{n}$, respectively.

Fig. 2) there are two possibilities as depicted in Fig. 3. Either the proton is able to go through the approaching SLAMS (denoted by 'escape' in Fig. 3a) or the proton is reflected and consequently returns to the shock transition (denoted by 'return' in Fig. 3b). The two protons in Fig. 3 started in a shock-SLAMS-system given by $b_m/b_0 = 2.0\,, \theta = 25^\circ\,, \psi = 0^\circ$ and $\theta_{vn} = 0^\circ$. The SLAMS approach the shock transition with $V_{SL} = 0.16$ and the particle starting velocities are $v_i = 3$ and $v_i = 6$ in Fig. 3a and 3b, respectively. Thus, the only difference between Fig. 3a and b is the magnitude of the starting velocity.

In general, the proton trajectories are influenced by six parameters (cf. Fig. 2): the magnetic field compression b_m within the SLAMS, the initial proton velocity v_i, the initial position of the SLAMS x_0, and the angles θ, ψ and θ_{vn}. In order to study under which conditions the proton initially reflected at the shock front returns towards the shock after its interaction with the SLAMS we analysed situations with three fixed parameters. In a first step we analysed proton trajectories for fixed magnetic field compression b_m, starting velocity v_i and starting angle θ_{vn} in a varying shock-SLAMS geometry, i.e., varying the angles ψ and θ (see Fig. 4). In each panel of Fig. 4 representing different magnetic field compressions we find regions, in which all protons starting at the transition zone with a fixed angle θ_{vn} are either reflected ('return') by the incoming SLAMS or go through them ('escape'). In the grey shaded regions the reflection behaviour depends on the starting position x_0 of the SLAMS. The location of the different kinds of regions is –for fixed b_m– determined by θ_{vn}. The width of the grey shaded area separating these regions is caused by the magnitude of the starting velocity, which causes different gyroradii $r_L := v_\perp/b$, with $v_\perp$ as particle velocity perpendicular to the local magnetic field b. As long as the particle's gyroradius is small in comparison with the length scale on which the magnetic field changes, i.e., $r_L|\nabla b/b| \ll 1$, the so-called adiabatic theory is applicable (e.g. Northrop 1963). According to this theory the reflection process at magnetic mirrors is purely determined by the particle's pitch angle $\alpha := \arctan(v_\perp/v_\parallel)$ ($v_\parallel$, particle velocity parallel to the local magnetic field). In each panel of Fig. 4 we show the theoretical computated dividing lines according to adiabatic theory for two different starting conditions $\theta_{vn} = 0^\circ$ and $\theta_{vn} = 30^\circ$. The dividing line for a quasi-parallel shock without incoming SLAMS ($\theta = 45^\circ$) is shown in the right half as a straight line. The parallel dotted line at $\theta = 39.9^\circ$ shows the region of shock-reencounter (Schwartz et al. 1983). The second dotted line ($\psi = \theta$) takes into account, that SLAMS exist within an angular range $0^\circ \le \psi \le \theta$.

The reflection condition in adiabatic theory can be obtained as follows (e.g. Krall & Trivelpiece 1986). For particles moving in smoothly varying magnetic fields and vanishing electric fields there are two constants of motion: the kinetic energy of the particle and the so-called "magnetic moment" defined by $m_M := v_\perp^2/b$. From this it follows that the particle is reflected if the pitch angle α of the particle is larger than the so-called loss-coss angle $\alpha_{lc} := \arcsin(b_0/b_{\max})^{1/2}$, with $b_{\max}$ as maximum value of the total magnetic field strength. In order to use this simple relationship one has to look for a frame of reference in which the electric field vanishes, the so-called de Hoffmann-Teller frame (de Hoffmann & Teller 1950). This frame can be found by setting $\boldsymbol{v}^{HT} = \boldsymbol{v} + \boldsymbol{V}_{HT}$ ($\boldsymbol{v}$ is the particle velocity in the shock rest frame), calculating the transformed electric field and requiring that the transformed electric field is equal to zero. Thus, using the Lorentz transformation formula for the electric field in first order of v/c the transformed electric field is given by $\boldsymbol{e}^{HT} = \boldsymbol{e} - \boldsymbol{V}_{HT} \times \boldsymbol{b}/c = 0$. Taking the magnetic field from Eq. 2 (with $p = 0$) and the electric field according to Eq. 3 (with $e_x = 0$) we obtain for the components of the de Hoffmann-Teller velocity

$$\begin{aligned} V_{HTx} &= V_{SL} \\ V_{HTy} &= 0 \\ V_{HTz} &= -V_{SH}\frac{\sin\theta}{\cos\psi} - V_{SL}\tan\psi\,. \end{aligned} \tag{5}$$

Furthermore, the reflection condition in the de Hoffmann-Teller frame can be written as

$$\alpha^{HT} := \arctan(v_\perp^{HT}/v_\parallel^{HT}) > \alpha_{lc}\,, \text{with}$$

$$\alpha_{lc} = \arcsin\left[\cos^2\psi + (\sin\psi + b_m)^2\right]^{-1/4}\,. \tag{6}$$

Since the velocities perpendicular and parallel to the magnetic field in the de Hoffmann-Teller frame contained in α^{HT} depend on trigonometrical functions of θ and ψ (cf. Eq. 5), we

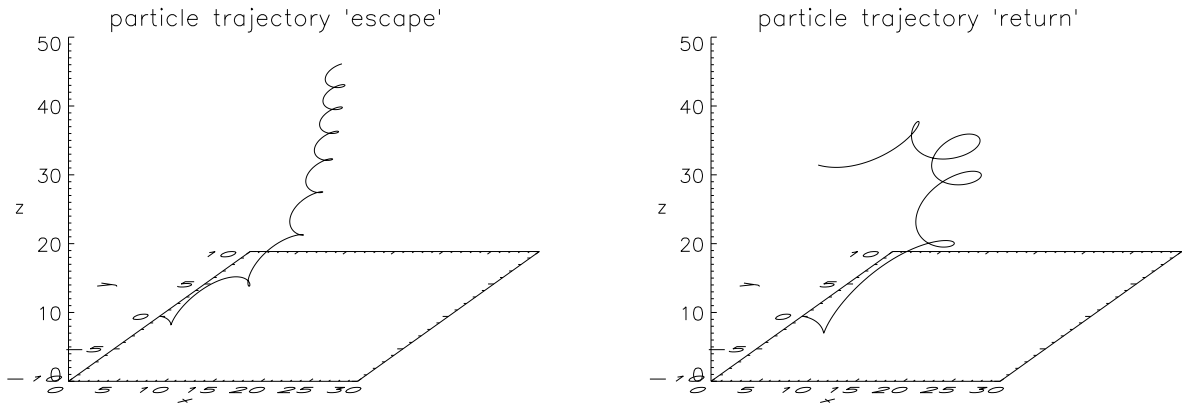

Fig. 3a and b. Test particle trajectories for protons starting with a velocity of **a** $v_i = 3$ and **b** $v_i = 6$ and an inclination of $\theta_{vn} = 0^\circ$. The global geometrical setup of the shock-SLAMS system is the same as in Fig. 2 and is specified by $\theta = 25^\circ$, $\psi = 0^\circ$, $b_m = 2.0$, and $x_0 = 25$. The proton from **a** is able to go through the approaching SLAMS, while the proton from **b** is reflected and returns to the shock transition.

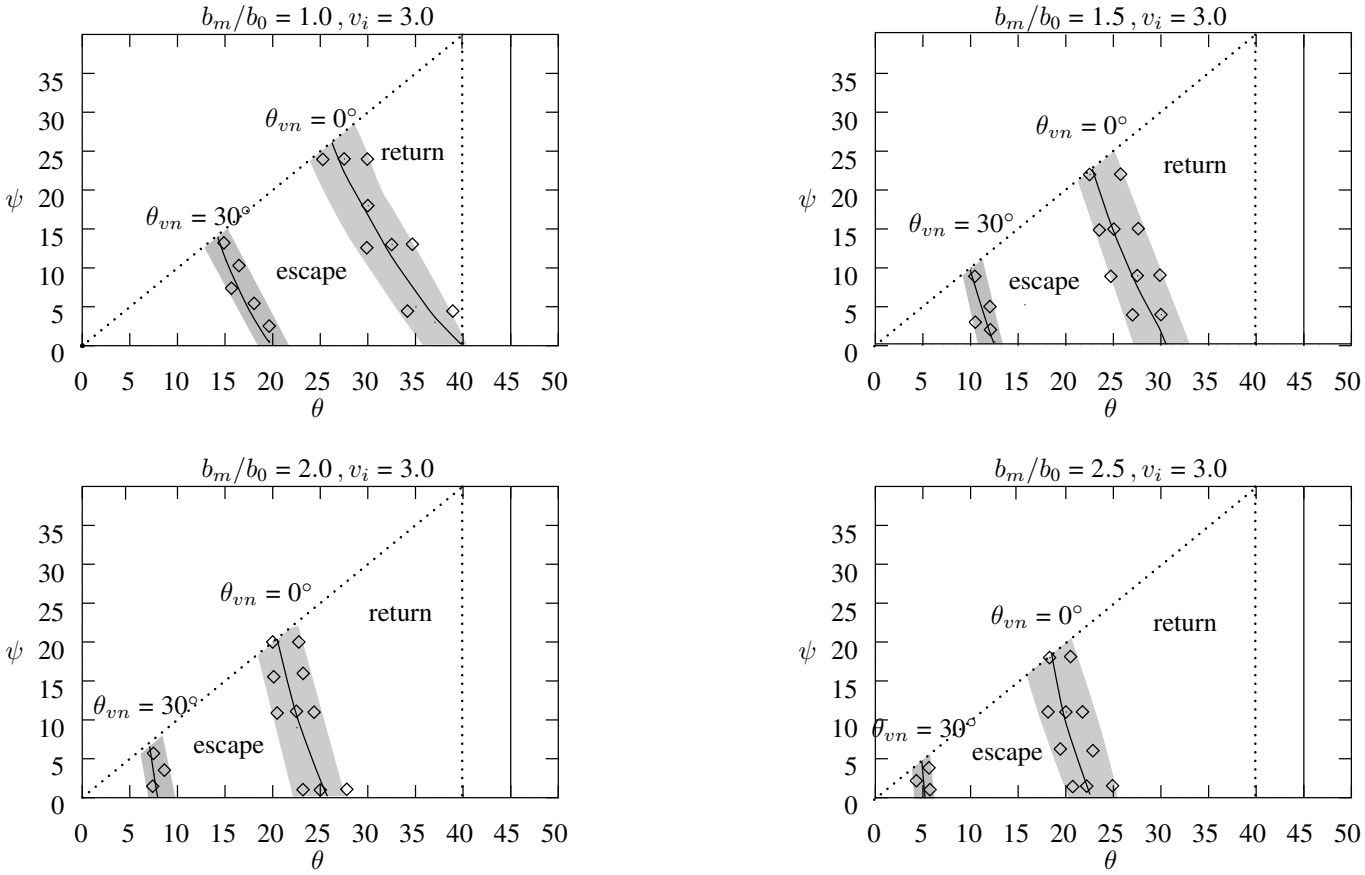

Fig. 4. Behaviour of protons starting at the shock transition zone with a velocity of $v_i = 3$ and inclinations of $\theta_{vn} = 0^\circ$ and $\theta_{vn} = 30^\circ$ at SLAMS with different magnetic field compressions. The regions marked by 'escape' and 'return' show the areas, in which all started protons either escape or return to the shock transition for $\theta_{vn} = 0^\circ$. In the grey shaded areas the proton behaviour depends on the starting position x_0 of the SLAMS. The curves and diamonds in these areas show computations according to adiabatic theory and results from our test particle calculations, respectively. The straight line at $\theta = 45^\circ$ is the dividing line for the 'escape-return' behaviour without magnetic field perturbations, the dotted line at $\theta = 39.9^\circ$ is the border line of shock-reencounter. The bisecting dotted line $\theta = \psi$ indicates the region in which SLAMS exist.

obtain a transcendental equation for the reflection condition. The theoretical curves in Fig. 4 (the lines in the grey shaded areas) were computed numerically from Eq. 6 for $\theta_{vn} = 0°$ and $\theta_{vn} = 30°$. The difference between the theoretical computed lines and the results from the test particle calculations are due to the fact that adiabatic theory is not valid for large gyroradii. The gyroradii for the proton trajectories depicted in Fig. 3 are about 2 and 4 times the ion inertial length for $v_i = 3$ and $v_i = 6$, respectively, while the scale length of the SLAMS are in the order of 10 ion inertial lengths. In this velocity ranges the proton behaviour depends not only on the geometrical starting conditions of the particle, i.e., θ_{vn}, but also on the specific conditions while entering the SLAMS.

The difference between the predictions of adiabatic theory and the effects of a finite gyroradius is also visible in Fig. 5, where we determined the magnetic field compression that is necessary for a reflection of the incoming protons. Fig. 5a shows the computated field compression corresponding to Eq. 6 for $\psi = 10°$ and $\theta_{vn} = 30°$ and the results of our test particle caculations for protons starting with a velocity of $v_i = 1.5$ for different values of x_0. Fig. 5b shows the adiabatic behaviour for $\psi = 10°$ and $\theta_{vn} = 0°$ and the test particle analysis for $v_i = 3$. Thus, Fig. 5 shows two different effects influencing the proton reflection process: Firstly, the geometric effect causing the location of the dotted lines. For protons starting nearly parallel, i.e., a small $\alpha = \arctan v_\perp/v_\parallel$, to the propagation direction of the SLAMS (Fig. 5b) we need a large magnetic field compression to reflect them. This becomes clear from Eq. 6, which shows that we need a large b_m to diminish α_{lc}. Secondly, the effect of a finite Larmor radius causes the different widths of the reflection zones in Fig. 5a and b. Furthermore, our test particle calculations showed, that the width for large starting velocities ($v_i > 10$) increases in such a way that the simple picture of two divided areas for reflection and transmission breaks down. On the other hand we find for the plasmas under consideration here, i.e., the plasma in the interplanetary medium, a normalized thermal proton velocity $v_{\rm therm}/V_A = (k_B T/m_p)^{1/2}/V_A$ in the order of 1, so that the velocity of slightly superthermal particles is smaller than 10.

In case of adiabatic particle behaviour the energy gained during the reflection process can be calculated using the aforementioned de Hoffmann-Teller frame. In the de Hoffmann-Teller frame the reflection process is described by $v_{r\parallel}^{HT} = -v_{i\parallel}^{HT}$ and $v_{r\perp}^{HT} = v_{i\perp}^{HT}$ (see e.g. Krall & Trivelpiece 1986). Thus, the transformation back into the shock rest frame leads to

$$v_{r\parallel} = -v_{i\parallel} + 2V_{SH}\frac{\sin\theta\sin\psi}{\cos\psi} + 2V_{SL}\sec\psi\,. \qquad (7)$$

The difference between the starting velocity and the velocity of the reflected proton parallel to the undisturbed magnetic field according to this equation obtained for $V_{SH} = 3.2$, $V_{SL} = 0.16$, $\theta = 21°$ and $\psi = 10°$ is $\Delta v_\parallel = |v_{r\parallel}| - |v_{i\parallel}| = 0.73$. On the other hand we found for the difference between the starting velocity and the mean velocity of the reflected protons parallel to the shock normal according to our test particle calculation a mean value of $\langle \Delta v_n \rangle = 0.61$ in good agreement with the theoretical expectations. Thus, Eq. 7 shows that the velocity gain (in the shock rest frame) is determined by the shock velocity and geometry on one hand (second term of the right side of Eq. 7) and by the velocity (third term) and the geometry (second and third term) of the approaching SLAMS.

4. Discussion

As already mentioned, the investigations presented in the previous section are closely related to an analysis of Fuselier et al. (1986). Before drawing a comparison between the results of these two papers and their application to the observations two brief remarks about the approach used in our paper should be made. The first one concerns the special shape used for our mathematically modelled SLAMS in Eq. 4. As can be seen from Eq. 6 the reflection behaviour in adiabatic theory is purely determined by the magnetic field compression and not by the particular shape of the reflecting mirror. The same statement holds for the velocity gain calculated in Eq. 7. These simple relations are modified as soon as the gyroradius of the ions under consideration becomes comparable to the scales L_1 or L_2. There are two possibilities for this modification: either a large wave steepening or a large gyroradius, i.e., a large kinetic energy of the incoming particle. The second remark is related to the standard theory of the first-order Fermi process using a diffusion-convection equation (e.g. Parker 1967). While this method is based on quasi-linear theory, i.e., small magnetic field fluctuations with $\delta B/B_0 \ll 1$ and a stochastical distribution, the approach in our paper starts with the opposite extreme, i.e., single, large amplitude fluctuations with $\delta B/B_0 > 1$. The finite amplitude waves or waves packets are additional, non-linear steps in the description of a simple first-order Fermi process. On the other hand Kang & Jones (1997) recently showed a good agreement between the continuum approach and Monte Carlo methods using test particles calculations in turbulent magnetic fields where it is assumed that the scattering process is elastic and keeps the velocity distribution isotropic.

The investigations carried out by Fuselier et al. (1986) refered to dependencies of the ion motion on wavelength, phase and amplitude of the waves convected into the shock. In our case the wavelength corresponds to the width of the SLAMS and the dependence on this width corresponds to the statement that the proton dynamics is influenced by the ratio of proton gyroradius and the scalelength of the reflecting mirror. The phase dependence mentioned by Fuselier et al. (1986) corresponds to the dependence of the starting position x_0. Furthermore, it should be emphasized that this "phase" (x_0 in our case) determines the probability of the SLAMS-reflected protons to penetrate into the downstream region.

Looking at the reflection condition from Eq. 6 it is not surprising that the proton behaviour depends on the magnetic field compression b_m of the reflecting mirror. On the other hand it is surprising that the adiabatic behaviour underlying Eq. 6 is still visible in Figs. 4 and 5. There may be two reasons for this rather simple reflection behaviour in comparison with the results found by Fuselier et al. (1986) (see e.g. Fig. 3 in their paper). Firstly, the protons are only occasionally affected by single

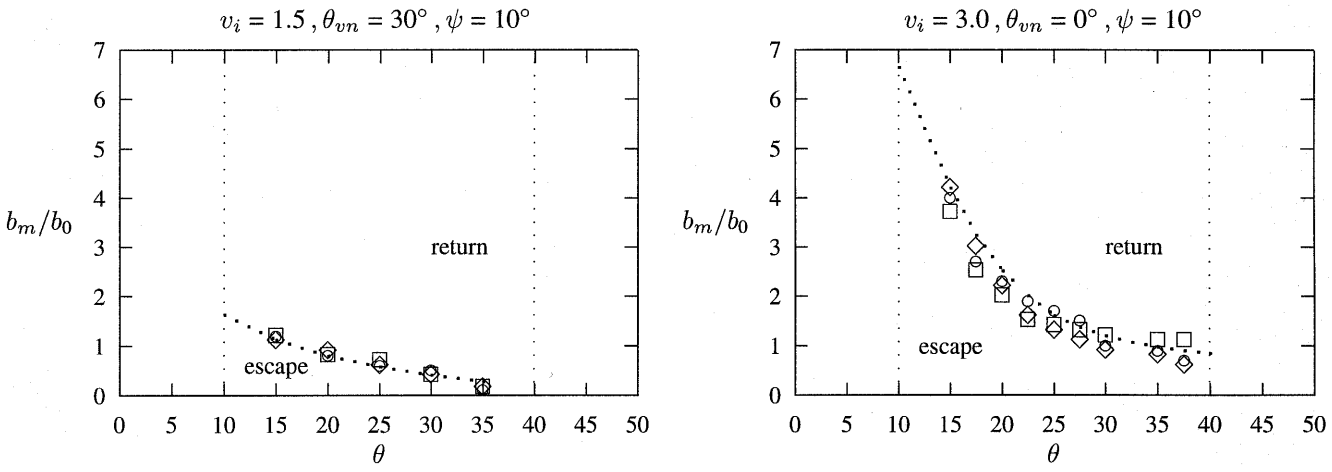

Fig. 5a and b. Proton behaviour at SLAMS with rising magnetic field compression b_m/b_0 in dependence from the angle θ for a fixed angle $\psi = 10°$. **a** 'escape-return' behaviour for $v_i = 1.5$ and $\theta_{vn} = 30°$ and **b** 'escape-return' behaviour for $v_i = 3.0$ and $\theta_{vn} = 0°$. The dotted lines show the computations for adiabatically moving particles and the different symbols show the results of our test particles computations for three different starting positions of the SLAMS (open squares: $x_0 = 25$, open circles: $x_0 = 30$, diamonds: $x_0 = 35$).

mirroring structures and for the rest of the time they move in a nearly undisturbed medium and secondly, the magnitude of the compression ratio is larger than the amplitude of the monochromatic MHD waves used by Fuselier et al. (1986). The influence of the magnitude of magnetic field compression on *non* adiabatic reflected particles can be obtained by a modification of the m_M-conserving reflection in Eq. 6. Assuming that the magnetic moment is changed about an amount δm_M this conservation law can be modified according to

$$\frac{w_\perp(0)}{b(0)} = \frac{w_\perp(t)}{b(t)} + \delta m_M(t)\,, \tag{8}$$

with $w_{\perp,\parallel}(t)$ as kinetic energy perpendicular and parallel to the local magnetic field $b(t)$ seen by the particle at the time t. From this equation and $w_\parallel(t) + w_\perp(t) = \text{const.}$ we obtain for the kinetic energy parallel to the local magnetic field

$$w_\parallel(t) = w_\parallel(0) + w_\perp(0)\left[1 - \frac{b(t)}{b(0)} + \frac{\delta m_M(t) b(t)}{w_\perp(0)}\right]\,. \tag{9}$$

Furthermore, the reflection condition can be obtained demanding $w_\parallel(t^*) = 0$ at a certain time t^*. Setting $\Delta m_M/m_M := \max(\delta m_M(t) b(t)/w_\perp(0))$ the modified reflection condition can be written as

$$\alpha^{HT} > \alpha_{lc}\,, \text{with}\;\; \alpha_{lc} = \arcsin\left(\frac{b_{max}}{b_0} + \frac{\Delta m_M}{m_M}\right)^{-1/2}\,. \tag{10}$$

In comparison to Eq. 6 this equation contains an additional term $\Delta m_M/m_M$. Thus, Eq. 10 illuminates, that the critical loss cone angle is fewer affected by $\Delta m_M/m_M$ for large values $b_{\max}/b_0$. For the calculations presented in this paper the value of $b_{\max}/b_0$ lies between 1 and 3, while the relative change of the magnetic moment $\Delta m_M/m_M$ is about 0.4 according to our test particle calculations with a ratio $r_L/L \approx 0.6$. This result is an good agreement with the theoretical considerations of Hellwig (1955) who showed that the magnetic moment is a constant at least to terms of order $(r_L/L)^2$. This result in connection with Eq. 10 explains the rather simple reflection behaviour in Fig. 4 and 5.

Furthermore, Figs. 4 and 5 show the following results: First, the presence of SLAMS in the upstream regions of quasi-parallel shocks prevents the protons reflected at the shock transition from escaping into the upstream region. With increasing magnetic field compression more and more ions are thrown back into the downstream direction and return with a larger energy than their starting energy (see Eq. 7). Thus, the dividing line at $\theta = 45°$ (see vertical line in Fig. 4) for shocks without upstream wave phenomena is shifted to smaller angles θ. The physical meaning of this result is an increase of available free energy in the downstream region, i.e., the upstream wave phenomena lead to a downstream heating. On the other hand it should be mentioned that the velocity change for test particles with a high starting velocity differs from the value computed by Eq. 7 which used the conservation of the magnetic moment. From this point of view the assumption of elastic scattering in the de Hoffmann-Teller frame is not trivial for large amplitude magnetic field fluctuations with a steep rise in the magnetic field.

Secondly, the simple reflection behaviour at single SLAMS depicted in Fig. 4 helps to understand the observations of coherent bunches of cold ions in the vicinity of the quasi-parallel bow shock. This means that as long as the ion velocity is not to high, e.g. $r_L/L < 0.3$ holds for $v_i < 3v_{\text{therm}}$ and means $\Delta m_M/m_M < 0.10$, these particles are reflected according to a rather simple reflection law (cf. Eq. 6). Furthermore, it becomes clear from Eq. 10 that a high magnetic field compression is rather insensitive to small changes in the magnetic moment during the reflection process. Thus, it seems natural to address the occasional presence of cold ion bunches to a reflection at the steepened waves structures investigated in the previous sections.

5. Summary

In our study we presented test particle calculations for superthermal protons under the influence of large magnetic field fluctuations at supercritical quasi-parallel shock waves. Due to the presence of these structures quasi-parallel shocks show features of quasi-perpendicular shocks, i.e., protons or ions reflected off the shock transition zone are prevented from escaping into the upstream region, they return to the transition zone and may penetrate into the downstream region with a superthermal energy and can thus contribute to downstream heating. The velocity gain can be computed according to Eq. 7.

In particular the following results were obtained: Describing SLAMS as reconvected simple MHD waves approaching the shock transition we found a dependence of the interacting protons on the magnetic field compression, the width, the direction and the starting position of the SLAMS. Fig. 4 showed, how far the dividing line between quasi-parallel and quasi-perpendicular shocks ($\theta_{B_0 n}$ = 45°) is shifted to smaller angles with rising magnetic field compression of SLAMS. The location of this line seperating regions of 'return'- and 'escape'-behaviour was calculated from numerical test particle calculations. These results were compared with analytical computations using adiabatic theory (Eq. 6). For a velocity range of $1.5V_{\rm therm} < v_i < 6V_{\rm therm}$ the deviation between numerical and analytical calculations are smaller than 30 %. In general the limits for an application of adiabatic theory depend on the ratio between the particle's gyroradius and the length scale of the reflecting structure. The magnetic moment is a constant up to the order $(r_L/L)^2$. Furthermore, a modified critical reflection angle for non adiabatic reflection was considered (Eq. 10).

In our analysis we followed closely the investigations of Fuselier et al. (1986), who made analogous studies for protons under the influence of finite amplitude, monochromatic MHD waves with a change in the magnetic field of $\Delta B/B \leq 1$. Doing so we broadened those results to large amplitude field fluctuations ($\Delta B/B \geq 1$) in the upstream region. We argued that the presence of these large amplitude field fluctuations enables us to understand the observations of cold ion bunches in a supercritical, quasi-parallel shock geometry.

References

Asbridge J.R., Bame S.J., Strong I.B., 1968, J.Geophys.Res., 73, 5777

Claßen H.-T., Mann G., 1997, A&A, 322, 696

de Hoffmann F., Teller E., 1950, Phys.Rev., 80, 692

Eastman T.E., Anderson R.R., Frank L.A., Parks G.K., 1981, J.Geophys.Res., 86, 4379

Fuselier S.A., Gosling J.T., Thomsen M.F., 1986, J.Geophys.Res., 91, 4163

Goodrich C. C., Scudder J.D., 1984, J.Geophys.Res., 89, A8, 6654

Gosling J.T., Asbridge J.R., Bame S.J., Paschmann G., Sckopke N., 1978, Geophys.Res.Lett., 5, 957

Gosling J.T., Thomsen M.F., Bame S.J., Feldmann W.C., Paschmann G., Sckopke N., 1982, Geophys.Res.Lett., 9, 1333

Gosling J.T., Thomsen M.F., Bame S.J., Russell C.T., 1989, J.Geophys.Res., 94, 10027

Hellwig G., 1955, Z.f.Naturforschung, 10a, 508

Hoppe M.M., Russell C.T., Frank L.A., Eastman T.E., Greenstadt E.W., 1981, J.Geophys.Res., 86, 4471

Kang H., Jones T.W., 1997, ApJ, 476, 875

Kennel C.F., Edmiston J.P., Hada T., 1985, in Stone R.G., Tsurutani B.T. (eds.) Collisionless Shocks in the Heliosphere: A Tutorial Review, AGU GN-34, Washington DC, p. 1

Krall N.A., Trivelpiece A.W., 1986, Principles of Plasma Physics, McGraw-Hill, New York

Kucharek H., Scholer M., 1991, J.Geophys.Res., 96, 21195

Malara F., Elaoufir J., 1991, J.Geophys.Res., 96, 7641

Mann G., 1995, J.Plasma.Phys., 53, 109

Mann G., Lühr H., Baumjohann W., 1994, J.Geophys.Res., 99, 13315

Northrop T.G., 1963, The Adiabatic Motion of Charged Particles, Wiley Interscience, New York

Omidi N., Winske D., 1990, J.Geophys.Res., 95, 2281

Onsager T.G., Thomsen M.F., Gosling J.T., Bame S.J., Russell C.T., 1990, J.Geophys.Res., 95, 2261

Parker E.N., 1967, Planet.Sp.Sci., 13, 9

Paschmann G., Sckopke N., Bame S.J., Asbridge J.R., Gosling J.T., Russell C.T., Greenstadt E.W., 1979, Geophys.Res.Lett., 6, 209

Paschmann G., Sckopke N., Bame S.J., Gosling J.T., 1982, Geophys.Res.Lett., 9, 881

Press W.H., Teukolsky S.A., Vetterling W.T., Flannery B.P., 1992, Numerical Recipes in Fortran: The Art of Scientific Computing, Cambridge

Russell C.T., Hoppe M.M., 1983, Space Sci.Rev., 34, 155

Scholer M., Fujimoto M., Kucharek H., 1992, ESA SP-346, 59

Schwartz S.J., Thomsen M.F., Gosling J.T., 1983, J.Geophys.Res., 88, 2039

Schwartz S.J., Burgess D., Wilkinson W.P., Kessel R.L., Dunlop M., Lühr H., 1992, J. Geophys. Res., 97, 4209

Sonnerup B.U.O., 1969, J.Geophys.Res., 74, 1301

Thomsen M.F., 1985, in Tsurutani B.T., Stone R.G. (eds.) Collisionless Shocks in the Heliosphere: Reviews of Current Research, AGU GN-34, Washington DC, p. 253

This article was processed by the author using Springer-Verlag LaTeX A&A style file *L-AA* version 3.